remote sensing

MDPI

Article

Rao and Wald Tests for Moving Target Detection in Forward Scatter Radar

Zeyu Wang [1,*], Hongmeng Chen [2], Yachao Li [3] and Dewu Wang [2]

[1] State Key Laboratory of Networking and Switching Technology, School of Information and Communication Engineering, Beijing University of Posts and Telecommunications, Beijing 100876, China
[2] Beijing Institute of Radio Measurement, Beijing 100854, China; chenhongmeng123@163.com (H.C.); wangdewu@bit.edu.cn (D.W.)
[3] National Laboratory of Radar Signal Processing, Xidian University, Xi'an 710071, China; ycli@mail.xidian.edu.cn
* Correspondence: zeyuwang@bupt.edu.cn

Abstract: This paper deals with adaptive moving target detection for a forward scatter radar in complex Gaussian noise. The echoes received by the forward scatter radar include not only the noise and the possible target signals but also the direct signals. To suppress the direct signals and detect the target signals, Rao and Wald tests are derived in two cases: the secondary data which contain no target signal are available or not available. Different from monostatic radar, it is proved that the derived Rao and Wald detectors for the forward scatter radar have the same test statistics as the generalized likelihood ratio test-based detector in the complex Gaussian noise both when the secondary data are available or not available. The numerical evaluation further demonstrates the equivalence and the effectiveness of the proposed detectors.

Keywords: adaptive detection; forward scatter radar; moving target; Rao test; Wald test

1. Introduction

A radar system in which the receiver is located separately from the transmitter is known as a bistatic radar [1–4]. When the bistatic angle, which represents an angle between the line of sight of the receiver antenna and the target and the line of sight of the transmitter antenna and the target, exceeds 135°, the receiver works in the forward scatter region of the target. In the forward scatter region of the target, the radar cross-section of the target increases with the bistatic angle and reaches its maximum when the bistatic angle becomes 180°. The forward scatter radar (FSR) is a bistatic radar with a bistatic angle close to 180° [5–8]. The forward scattering makes the FSR system have an enhanced radar cross-section compared with monostatic radar system. Moreover, the forward scattering cross-section is independent of the material of the target. Therefore, FSR geometry has received extensive attention in the fields of target motion parameter estimation, passive FSR, target localization, target classification, and target detection in recent years [9–11].

For target motion parameter estimation, the method to estimate the target velocity, target position, and crossing time is discussed in [12,13] in a global navigation satellite system-based FSR network. Based on single-baseline and dual-baseline FSR configurations, closed-form expressions of Cramer–Rao bounds of the target motion parameters are given in [11]. For passive FSR, the matched filter and linear canonical transformation are used to realize aerial target passive sensing with satellite-based FSR in [14]. The ability of a digital video broadcasting terrestrial-based passive FSR to detect targets is discussed in [15,16]. For target localization, the maximum likelihood estimation (MLE) method for locating a moving target in FSR is discussed in [17]. For target classification, a neural network classifier was designed to classify ground targets using FSR in [18].

Citation: Wang, Z.; Chen, H.; Li, Y.; Wang, D. Rao and Wald Tests for Moving Target Detection in Forward Scatter Radar. *Remote Sens.* **2024**, *16*, 211. https://doi.org/10.3390/rs16020211

Academic Editor: Shuying Li

Received: 22 November 2023
Revised: 21 December 2023
Accepted: 3 January 2024
Published: 5 January 2024

Target detection is one of the most important applications of FSR [11]. In Ref. [19], a stationary and slow-moving target detection scheme is proposed for a novel FSR system in which the transmitter is rotated. By using this novel FSR system and the proposed target detection scheme, stationary and crawling human intruders can be detected. In Ref. [20], matched filtering theory is utilized to maximize signal-to-noise ratio for ground target detection through forward scatter micro radars. In Ref. [21], the theoretical performance of a crystal video detector (CVD) scheme which consists of the squared modulus operation, a narrow high-pass filter, and a matched filter is derived. The comparison of the CVD with the ideal detector shows that the CVD undergoes detection performance losses under the condition that the target approaches the near field. To improve the detection performance, adaptive detectors for FSR were designed by utilizing the generalized likelihood ratio test (GLRT) when the parameters of direct signal, target signal, and noise are partly known and completely unknown in [22]. The new detectors can achieve more than 3 dB detection performance improvement than the CVD.

The GLRT is one of the most widely used design criteria for the adaptive detector, which is designed by jointly utilizing the primary data and the secondary data and is compared with a detection threshold set according to a pre-assigned probability of false alarm to decide whether the target exists [23–26]. However, the GLRT does not generally have optimality properties in the finite-sample case. Apart from GLRT, the Rao test and Wald test are alternative design criteria that are asymptotically equal to the GLRT. The adaptive detectors designed according to the Rao test and Wald test may achieve better detection performance than the GLRT in the finite-sample case [27–31]. Therefore, it is of interest to investigate the behavior of the adaptive detectors derived according to the Rao and Wald tests. Both the Rao and Wald tests have been applied in different signal detection scenarios [32–34]. In Ref. [35], the subspace Wald and GLRT detectors are proposed to deal with the signal mismatch problem in MIMO radar. The resulting Wald test is more robust than the GLRT. Considering that some training data may contain jamming, adaptive GLRT, Rao, and Wald tests are designed in noise, clutter, and noise cover pulse jamming in [36]. Persymmetric Wald and GLRT detectors were designed to detect spread spectrum signals in noise in [37]. The proposed Wald test was found to share the same decision rule with the proposed GLRT. To detect point-like targets in a complex Gaussian environment, modified Durbin, Wald, and Rao detectors were designed in [38] by replacing the exact Fisher information matrix (FIM) with its estimator. To detect radar targets in non-Gaussian and nonhomogeneous sea clutter, persymmetric Wald, Rao, and GLRT detectors are derived in [39]. However, as far as the authors know, no work has discussed the design of adaptive Rao and Wald detectors for FSR.

In this paper, adaptive moving target detection for FSR in complex Gaussian noise is discussed. The contributions of the paper are three-fold. (1) Adaptive detectors which can realize the direct signal suppression and target detection simultaneously are designed for the FSR by resorting to the Rao and Wald design criteria. Rather than using the imaginary and real parts of the complex parameter to derive the real parameter test statistics, four adaptive target detectors are proposed by regarding the complex parameter as a whole. (2) The equivalence of GLRT, Rao, and Wald detectors based on FSR for a finite amount of data is demonstrated through both theoretical analysis and Monte Carlo simulations when the secondary data are available and not available. (3) Our simulation results show that the proposed Rao and Wald detectors outperform their counterpart and that the detection performance of the proposed Rao and Wald detectors increases when the observation time and the number of the secondary data increase are provided.

We have arranged the rest of this paper as follows. Adaptive Rao and Wald detectors for the FSR were designed for when the secondary data are available and not available in Sections 2 and 3. The equivalence of the Wald test and Rao test to the GLRT is proved in Section 4. The detection performance analysis of the derived adaptive detectors is shown in Section 5. Some conclusions are given in Section 6.

2. Design of Adaptive Detectors with Secondary Data

Adaptive moving rectangular-shaped target detection in complex Gaussian noise using the FSR is considered. As shown in Figure 1, the length of the baseline between the receiver and the transmitter of the FSR is R. The transmitter transmits a continuous wave signal with carrier frequency f_c. A target with vertical dimension L_v and horizontal dimension L_h moves in a straight line with velocity v and crosses the baseline at a distance R_0 from the receiver when $t = 0$ s.

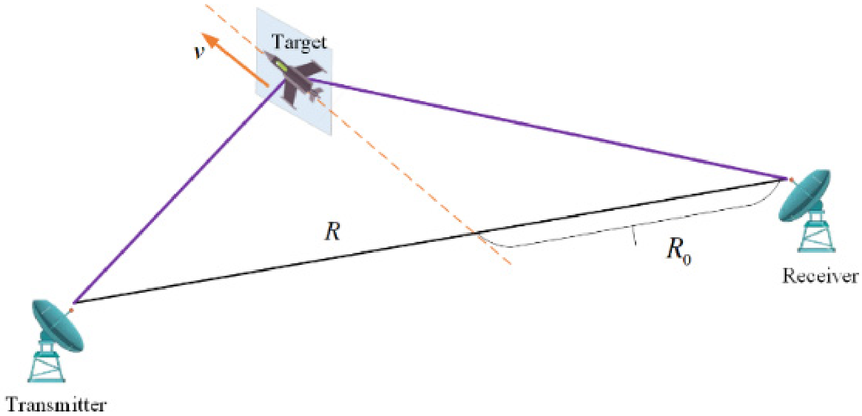

Figure 1. The geometry of the forward scatter radar.

When the secondary data are available, we formulate the above detection problem as the binary hypothesis test

$$\begin{cases} H_0 : \begin{cases} \boldsymbol{z} = \alpha \boldsymbol{r}_d + \boldsymbol{n} \\ \boldsymbol{z}' = \alpha \boldsymbol{r}'_d + \boldsymbol{n}' \end{cases} \\ H_1 : \begin{cases} \boldsymbol{z} = \alpha \boldsymbol{r}_d + \beta \boldsymbol{r}_t + \boldsymbol{n} \\ \boldsymbol{z}' = \alpha \boldsymbol{r}'_d + \boldsymbol{n}' \end{cases} \end{cases} \tag{1}$$

where H_0 denotes the null hypothesis indicating the absence of the target signal, H_1 denotes the alternative hypothesis indicating the presence of the target signal, $\boldsymbol{z} \in \mathbb{C}_{N\times1}$ denotes the data under test, namely, the primary data, $\mathbb{C}_{N\times1}$ stands for the set of N -dimensional complex vectors, $\boldsymbol{z}' \in \mathbb{C}_{K\times1}$ denotes the secondary data which are target-free and are collected from the temporal frames adjacent to the primary data, $\boldsymbol{r}_d \in \mathbb{C}_{N\times1}$ and $\boldsymbol{r}'_d \in \mathbb{C}_{K\times1}$ denote complex vectors containing samples collected from the direct signals, $\boldsymbol{r}_t \in \mathbb{C}_{N\times1}$ denotes the N -dimensional complex vector containing samples collected from the target signal, β and α are unknown complex amplitudes of the target signal and direct signal, $\boldsymbol{n} \in \mathbb{C}_{N\times1}$ and $\boldsymbol{n}' \in \mathbb{C}_{K\times1}$ denote the noise which satisfies $\boldsymbol{n} \sim \mathcal{CN}(\boldsymbol{0}, \sigma^2 \boldsymbol{I}_N), \boldsymbol{n}' \sim \mathcal{CN}(\boldsymbol{0}, \sigma^2 \boldsymbol{I}_K)$, σ^2 denotes the noise variance, $\boldsymbol{I}_N$ and $\boldsymbol{I}_K$ denote the identity matrices, and $\mathcal{CN}(\cdot)$ denotes complex circular symmetric Gaussian distribution. According to the statistical distributions of the target signal, direct signal, and noise, the joint probability density function (JPDF) of $\boldsymbol{z}$ and $\boldsymbol{z}'$ is

$$f(\boldsymbol{z}, \boldsymbol{z}'|H_i) = \frac{1}{\pi^{(N+K)}\sigma^{2(N+K)}} \exp\left[-\frac{1}{\sigma^2}\left(\|\boldsymbol{z} - \alpha \boldsymbol{r}_d - i\beta \boldsymbol{r}_t\|^2 + \|\boldsymbol{z}' - \alpha \boldsymbol{r}'_d\|^2\right)\right] \tag{2}$$

where $i = 0,\ 1$, $\|\cdot\|$ is the Euclidean norm.

Compared with the GLRT, which is obtained by estimating unknown parameters under both hypothesis H_0 and hypothesis H_1, only the unknown parameters under hypothesis H_0 or the unknown parameters under hypothesis H_1 are required to estimate for the Rao test or the Wald test. Meanwhile, considering that the complex-parameter Rao and Wald tests coincide with the real-parameter ones [28], and that the real-parameter Rao and Wald tests may be difficult to handle and have heavy computational complexity, we regard the complex parameter as a whole to design the Rao and Wald detectors for FSR in this section.

2.1. Adaptive Complex Parameter Rao Detector with Secondary Data

The complex parameter Rao test with secondary data for the detection problem (1) is

$$\left.\frac{\partial \ln f(z,z'|H_1)}{\partial \Theta_r}\right|^T_{\Theta=\hat{\Theta}_0}\left[J^{-1}(\hat{\Theta}_0)\right]_{\Theta_r\Theta_r}\left.\frac{\partial \ln f(z,z'|H_1)}{\partial \Theta_r^*}\right|_{\Theta=\hat{\Theta}_0}\underset{H_0}{\overset{H_1}{\gtrless}}\gamma \tag{3}$$

where $\ln(\cdot)$ denotes the logarithm, $(\cdot)^T$ and $(\cdot)^*$ are the transpose operator and the complex conjugate operator, $\partial(\cdot)$ denotes the partial derivative, γ denotes the detection threshold, $\Theta = \left[\Theta_r^T, \Theta_s^T\right]^T$, $\Theta_r = \left[\beta^T, \beta^H\right]^T$ is the vector of the relevant parameter which is related to the complex amplitude of the target signal, $\Theta_s = \left[\alpha^T, \alpha^H, \sigma^2\right]^T$ is the vector of nuisance parameters, which include the complex amplitude of direct signal and the noise variance, $(\cdot)^H$ is the complex conjugate transpose operator, $\hat{\Theta}_0$ denotes the MLE of Θ under H_0, and $J(\Theta)$ is the FIM:

$$\begin{aligned} J(\Theta) &= E\left[\frac{\partial \ln f(z,z'|H_1)}{\partial \Theta^*}\frac{\partial \ln f(z,z'|H_1)}{\partial \Theta^T}\right] \\ &= \begin{bmatrix} J_{\Theta_r\Theta_r} & J_{\Theta_r\Theta_s} \\ J_{\Theta_s\Theta_r} & J_{\Theta_s\Theta_s} \end{bmatrix} \end{aligned} \tag{4}$$

where $J_{\Theta_r\Theta_r}$, $J_{\Theta_r\Theta_s}$, $J_{\Theta_s\Theta_r}$, and $J_{\Theta_s\Theta_s}$ are four blocks of $J(\Theta)$:

$$J_{\Theta_r\Theta_r} = E\left[\frac{\partial \ln f(z,z'|H_1)}{\partial \Theta_r^*}\frac{\partial \ln f(z,z'|H_1)}{\partial \Theta_r^T}\right] \tag{5}$$

$$J_{\Theta_r\Theta_s} = E\left[\frac{\partial \ln f(z,z'|H_1)}{\partial \Theta_r^*}\frac{\partial \ln f(z,z'|H_1)}{\partial \Theta_s^T}\right] \tag{6}$$

$$J_{\Theta_s\Theta_r} = J^H_{\Theta_r\Theta_s} \tag{7}$$

$$J_{\Theta_s\Theta_s} = E\left[\frac{\partial \ln f(z,z'|H_1)}{\partial \Theta_s^*}\frac{\partial \ln f(z,z'|H_1)}{\partial \Theta_s^T}\right] \tag{8}$$

$\left[J^{-1}(\Theta)\right]_{\Theta_r\Theta_r}$ is the (Θ_r, Θ_r) part of the inverse of the matrix $J(\Theta)$. According to the inverse formula of partitioned matrices, we have

$$\left[J^{-1}(\Theta)\right]_{\Theta_r\Theta_r} = \left[J_{\Theta_r\Theta_r}(\Theta) - J_{\Theta_r\Theta_s}(\Theta)J^{-1}_{\Theta_s\Theta_s}(\Theta)J_{\Theta_s\Theta_r}(\Theta)\right]^{-1} \tag{9}$$

To obtain the Rao test, we express the partial derivative of the logarithm of the JPDF $\ln f(z,z'|H_1)$ to Θ_r as

$$\frac{\partial \ln f(z,z'|H_1)}{\partial \Theta_r^T} = \left[\frac{\partial \ln f(z,z'|H_1)}{\partial \Theta_r^*}\right]^H = \begin{bmatrix} \frac{\partial \ln f(z,z'|H_1)}{\partial \beta^*} \\ \frac{\partial \ln f(z,z'|H_1)}{\partial \beta} \end{bmatrix}^H \tag{10}$$

Substituting (2) into (10), we have:

$$\frac{\partial \ln f(z,z'|H_1)}{\partial \beta^*} = \frac{1}{\sigma^2}\left(r_t^H z - \alpha r_t^H r_d - \beta r_t^H r_t\right) \tag{11}$$

$$\frac{\partial \ln f(z,z'|H_1)}{\partial \beta} = \frac{1}{\sigma^2}\left(z^H r_t - \alpha^H r_d^H r_t - \beta^H r_t^H r_t\right) \tag{12}$$

The FIM $\boldsymbol{J}(\Theta)$ is calculated according to the JPDF $f(\boldsymbol{z},\boldsymbol{z}'|H_1)$ (2) and the theory of complex-valued matrix differentiation [40]. After some calculation, we obtain:

$$\frac{\partial^2 \ln f_1}{\partial \beta^* \partial \beta^T} = -\frac{1}{\sigma^2}\boldsymbol{r}_t^H\boldsymbol{r}_t \tag{13}$$

$$\frac{\partial^2 \ln f_1}{\partial \beta \partial \beta^H} = -\frac{1}{\sigma^2}\boldsymbol{r}_t^H\boldsymbol{r}_t \tag{14}$$

$$\frac{\partial^2 \ln f_1}{\partial \beta \partial \beta^T} = 0 \tag{15}$$

$$\frac{\partial^2 \ln f_1}{\partial \beta^* \partial \beta^H} = 0 \tag{16}$$

where $f_1 = f(\boldsymbol{z},\boldsymbol{z}'|H_1)$. Since the equation $E\left[\frac{\partial \ln f}{\partial A}\frac{\partial \ln f}{\partial B}\right] = -E\left[\frac{\partial^2 \ln f}{\partial A \partial B}\right] = -E\left[\frac{\partial}{\partial B}\left(\frac{\partial \ln f}{\partial A}\right)\right]$ holds, we can obtain the first block $\boldsymbol{J}_{\Theta_r\Theta_r}$:

$$\begin{aligned}\boldsymbol{J}_{\Theta_r\Theta_r} &= E\left[\frac{\partial \ln f(\boldsymbol{z},\boldsymbol{z}'|H_1)}{\partial \Theta_r^*}\frac{\partial \ln f(\boldsymbol{z},\boldsymbol{z}'|H_1)}{\partial \Theta_r^T}\right] \\ &= E\begin{bmatrix} \frac{\partial \ln f_1}{\partial \beta^*}\frac{\partial \ln f_1}{\partial \beta^T} & \frac{\partial \ln f_1}{\partial \beta^*}\frac{\partial \ln f_1}{\partial \beta^H} \\ \frac{\partial \ln f_1}{\partial \beta}\frac{\partial \ln f_1}{\partial \beta^T} & \frac{\partial \ln f_1}{\partial \beta}\frac{\partial \ln f_1}{\partial \beta^H} \end{bmatrix} \\ &= \begin{bmatrix} \frac{1}{\sigma^2}\boldsymbol{r}_t^H\boldsymbol{r}_t & 0 \\ 0 & \frac{1}{\sigma^2}\boldsymbol{r}_t^H\boldsymbol{r}_t \end{bmatrix}\end{aligned} \tag{17}$$

In a similar way, we can obtain

$$\frac{\partial^2 \ln f_1}{\partial \beta^* \partial \alpha^T} = -\frac{1}{\sigma^2}\boldsymbol{r}_t^H\boldsymbol{r}_d \tag{18}$$

$$\frac{\partial^2 \ln f_1}{\partial \beta^* \partial \sigma^2} = -\left(\frac{1}{\sigma^2}\right)^2\left(\boldsymbol{r}_t^H\boldsymbol{z} - \alpha\boldsymbol{r}_t^H\boldsymbol{r}_d - \beta\boldsymbol{r}_t^H\boldsymbol{r}_t\right) \tag{19}$$

$$\frac{\partial^2 \ln f_1}{\partial \beta^* \partial \alpha^H} = 0 \tag{20}$$

$$\frac{\partial^2 \ln f_1}{\partial \beta \partial \alpha^H} = -\frac{1}{\sigma^2}\boldsymbol{r}_d^H\boldsymbol{r}_t \tag{21}$$

$$\frac{\partial^2 \ln f_1}{\partial \beta \partial \sigma^2} = -\left(\frac{1}{\sigma^2}\right)^2\left(\boldsymbol{z}^H\boldsymbol{r}_t - \alpha^H\boldsymbol{r}_d^H\boldsymbol{r}_t - \beta^H\boldsymbol{r}_t^H\boldsymbol{r}_t\right) \tag{22}$$

$$\frac{\partial^2 \ln f_1}{\partial \beta \partial \alpha^T} = 0 \tag{23}$$

Then, the second block $\boldsymbol{J}_{\Theta_r\Theta_s}$ can be calculated as follows:

$$\begin{aligned}\boldsymbol{J}_{\Theta_r\Theta_s} &= E\left[\frac{\partial \ln f(\boldsymbol{z},\boldsymbol{z}'|H_1)}{\partial \Theta_r^*}\frac{\partial \ln f(\boldsymbol{z},\boldsymbol{z}'|H_1)}{\partial \Theta_s^T}\right] \\ &= E\begin{bmatrix} \frac{\partial \ln f_1}{\partial \beta^*}\frac{\partial \ln f_1}{\partial \alpha^T} & \frac{\partial \ln f_1}{\partial \beta^*}\frac{\partial \ln f_1}{\partial \alpha^H} & \frac{\partial \ln f_1}{\partial \beta^*}\frac{\partial \ln f_1}{\partial \sigma^2} \\ \frac{\partial \ln f_1}{\partial \beta}\frac{\partial \ln f_1}{\partial \alpha^T} & \frac{\partial \ln f_1}{\partial \beta}\frac{\partial \ln f_1}{\partial \alpha^H} & \frac{\partial \ln f_1}{\partial \beta}\frac{\partial \ln f_1}{\partial \sigma^2} \end{bmatrix} \\ &= \begin{bmatrix} \frac{1}{\sigma^2}\boldsymbol{r}_t^H\boldsymbol{r}_d & 0 & 0 \\ 0 & \frac{1}{\sigma^2}\boldsymbol{r}_d^H\boldsymbol{r}_t & 0 \end{bmatrix}\end{aligned} \tag{24}$$

According to the definition of the block $\boldsymbol{J}_{\Theta_s\Theta_s}$, we have the following results:

$$\frac{\partial^2 \ln f_1}{\partial \alpha^* \partial \alpha^T} = -\frac{1}{\sigma^2}\left(\boldsymbol{r}_d^H \boldsymbol{r}_d + \boldsymbol{r}_d'^H \boldsymbol{r}_d'\right) \tag{25}$$

$$\frac{\partial^2 \ln f_1}{\partial \alpha^* \partial \alpha^H} = 0 \tag{26}$$

$$\frac{\partial^2 \ln f_1}{\partial \alpha^* \partial \sigma^2} = -\left(\frac{1}{\sigma^2}\right)^2 \left(\boldsymbol{r}_d^H \boldsymbol{z} - \alpha \boldsymbol{r}_d^H \boldsymbol{r}_d - \beta \boldsymbol{r}_d^H \boldsymbol{r}_t + \boldsymbol{r}_d'^H \boldsymbol{z}' - \alpha \boldsymbol{r}_d'^H \boldsymbol{r}_d'\right) \tag{27}$$

$$\frac{\partial^2 \ln f_1}{\partial \alpha \partial \alpha^T} = 0 \tag{28}$$

$$\frac{\partial^2 \ln f_1}{\partial \alpha \partial \alpha^H} = -\frac{1}{\sigma^2}\left(\boldsymbol{r}_d^H \boldsymbol{r}_d + \boldsymbol{r}_d'^H \boldsymbol{r}_d'\right) \tag{29}$$

$$\frac{\partial^2 \ln f_1}{\partial \alpha \partial \sigma^2} = -\left(\frac{1}{\sigma^2}\right)^2 \left(\boldsymbol{z}^H \boldsymbol{r}_d - \alpha^H \boldsymbol{r}_d^H \boldsymbol{r}_d - \beta^H \boldsymbol{r}_t^H \boldsymbol{r}_d + \boldsymbol{z}'^H \boldsymbol{r}_d' - \alpha^H \boldsymbol{r}_d'^H \boldsymbol{r}_d'\right) \tag{30}$$

$$\frac{\partial^2 \ln f_1}{\partial \sigma^2 \partial \alpha^T} = -\left(\frac{1}{\sigma^2}\right)^2 \left(\boldsymbol{z}^H \boldsymbol{r}_d - \alpha^H \boldsymbol{r}_d^H \boldsymbol{r}_d - \beta^H \boldsymbol{r}_t^H \boldsymbol{r}_d + \boldsymbol{z}'^H \boldsymbol{r}_d' - \alpha^H \boldsymbol{r}_d'^H \boldsymbol{r}_d'\right) \tag{31}$$

$$\frac{\partial^2 \ln f_1}{\partial \sigma^2 \partial \alpha^H} = -\left(\frac{1}{\sigma^2}\right)^2 \left(\boldsymbol{r}_d^H \boldsymbol{z} - \alpha \boldsymbol{r}_d^H \boldsymbol{r}_d - \beta \boldsymbol{r}_d^H \boldsymbol{r}_t + \boldsymbol{r}_d'^H \boldsymbol{z}' - \alpha \boldsymbol{r}_d'^H \boldsymbol{r}_d'\right) \tag{32}$$

$$\frac{\partial^2 \ln f_1}{\partial \sigma^2 \partial \sigma^2} = (N+K)\left(\frac{1}{\sigma^2}\right)^2 - 2\left(\frac{1}{\sigma^2}\right)^3 \left(\|\boldsymbol{z} - \alpha \boldsymbol{r}_d - i\beta \boldsymbol{r}_t\|^2 + \left\|\boldsymbol{z}' - \alpha \boldsymbol{r}_d'\right\|^2\right) \tag{33}$$

$$\begin{aligned}
\boldsymbol{J}_{\Theta_s\Theta_s} &= E\left[\frac{\partial \ln f(\boldsymbol{z},\boldsymbol{z}'|H_1)}{\partial \Theta_s^*}\frac{\partial \ln f(\boldsymbol{z},\boldsymbol{z}'|H_1)}{\partial \Theta_s^T}\right] \\
&= E\begin{bmatrix}
\frac{\partial \ln f_1}{\partial \alpha^*}\frac{\partial \ln f_1}{\partial \alpha^T} & \frac{\partial \ln f_1}{\partial \alpha^*}\frac{\partial \ln f_1}{\partial \alpha^H} & \frac{\partial \ln f_1}{\partial \alpha^*}\frac{\partial \ln f_1}{\partial \sigma^2} \\
\frac{\partial \ln f_1}{\partial \alpha}\frac{\partial \ln f_1}{\partial \alpha^T} & \frac{\partial \ln f_1}{\partial \alpha}\frac{\partial \ln f_1}{\partial \alpha^H} & \frac{\partial \ln f_1}{\partial \alpha}\frac{\partial \ln f_1}{\partial \sigma^2} \\
\frac{\partial \ln f_1}{\partial \sigma^2}\frac{\partial \ln f_1}{\partial \alpha^T} & \frac{\partial \ln f_1}{\partial \sigma^2}\frac{\partial \ln f_1}{\partial \alpha^H} & \frac{\partial \ln f_1}{\partial \sigma^2}\frac{\partial \ln f_1}{\partial \sigma^2}
\end{bmatrix} \\
&= \frac{1}{\sigma^2}\begin{bmatrix}
\left(\boldsymbol{r}_d^H \boldsymbol{r}_d + \boldsymbol{r}_d'^H \boldsymbol{r}_d'\right) & 0 & 0 \\
0 & \left(\boldsymbol{r}_d^H \boldsymbol{r}_d + \boldsymbol{r}_d'^H \boldsymbol{r}_d'\right) & 0 \\
0 & 0 & \frac{(N+K)}{\sigma^2}
\end{bmatrix}
\end{aligned} \tag{34}$$

$\left[\boldsymbol{J}^{-1}(\Theta)\right]_{\Theta_r\Theta_r}$ can be obtained by substituting (17), (24), and (34) into (9):

$$\begin{aligned}
&\left[\boldsymbol{J}^{-1}(\Theta)\right]_{\Theta_r\Theta_r} \\
&= \left[\boldsymbol{J}_{\Theta_r\Theta_r}(\Theta) - \boldsymbol{J}_{\Theta_r\Theta_s}(\Theta)\boldsymbol{J}_{\Theta_s\Theta_s}^{-1}(\Theta)\boldsymbol{J}_{\Theta_s\Theta_r}(\Theta)\right]^{-1} \\
&= \sigma^2\left[\|\boldsymbol{r}_t\|^2 - \frac{\boldsymbol{r}_t^H \boldsymbol{r}_d \boldsymbol{r}_d^H \boldsymbol{r}_t}{\left(\|\boldsymbol{r}_d\|^2 + \left\|\boldsymbol{r}_d'\right\|^2\right)}\right]^{-1} \boldsymbol{I}_2
\end{aligned} \tag{35}$$

The MLEs of the unknown parameters under H_0 is: $\hat{\beta}_0 = 0$, $\hat{\alpha}_0 = \left(\|\boldsymbol{r}_d\|^2 + \left\|\boldsymbol{r}_d'\right\|^2\right)^{-1}\left(\boldsymbol{r}_d^H \boldsymbol{z} + \boldsymbol{r}_d'^H \boldsymbol{z}'\right)$, $\hat{\sigma}_0^2 = \frac{1}{(N+K)}\left[\|\boldsymbol{z}\|^2 + \|\boldsymbol{z}'\|^2 - \frac{\left|\left(\boldsymbol{r}_d^H \boldsymbol{z} + \boldsymbol{r}_d'^H \boldsymbol{z}'\right)\right|^2}{\|\boldsymbol{r}_d\|^2 + \left\|\boldsymbol{r}_d'\right\|^2}\right]$.

The complex parameter Rao test with secondary data based on the FSR (referred to as Rao-SD-FSR) can be obtained by substituting (10)–(35) and the MLEs of the unknown parameters under H_0 into (3):

$$T_{Rao-SD-FSR} = \frac{\left|\boldsymbol{r}_t^H\left[\boldsymbol{z} - \frac{\boldsymbol{r}_d\left(\boldsymbol{r}_d^H \boldsymbol{z} + \boldsymbol{r}_d'^H \boldsymbol{z}'\right)}{\|\boldsymbol{r}_d\|^2 + \left\|\boldsymbol{r}_d'\right\|^2}\right]\right|^2 \Big/ \left(\|\boldsymbol{r}_t\|^2 - \frac{\boldsymbol{r}_t^H \boldsymbol{r}_d \boldsymbol{r}_d^H \boldsymbol{r}_t}{\|\boldsymbol{r}_d\|^2 + \left\|\boldsymbol{r}_d'\right\|^2}\right)}{\|\boldsymbol{z}\|^2 + \|\boldsymbol{z}'\|^2 - \frac{\left|\left(\boldsymbol{r}_d^H \boldsymbol{z} + \boldsymbol{r}_d'^H \boldsymbol{z}'\right)\right|^2}{\|\boldsymbol{r}_d\|^2 + \left\|\boldsymbol{r}_d'\right\|^2}} \underset{H_0}{\overset{H_1}{\gtrless}} \gamma' \tag{36}$$

where γ' denotes the modified detection threshold.

2.2. Adaptive Complex Parameter Wald Detector with Secondary Data

The complex parameter Wald test with secondary data is given by

$$\left(\hat{\Theta}_{r1}-\Theta_{r0}\right)^H\left\{\left[\boldsymbol{J}^{-1}\left(\hat{\Theta}_1\right)\right]_{\Theta_r\Theta_r}\right\}^{-1}\left(\hat{\Theta}_{r1}-\Theta_{r0}\right)\underset{H_0}{\overset{H_1}{\gtrless}}\eta \tag{37}$$

where $\hat{\Theta}_1$ and $\hat{\Theta}_{r1}$ are the MLEs of Θ and Θ_r under H_1, η denotes the detection threshold, and Θ_{r0} is the value of Θ_r under H_0.

From (35), $\left\{\left[\boldsymbol{J}^{-1}(\Theta)\right]_{\Theta_r\Theta_r}\right\}^{-1}$ is calculated as:

$$\begin{aligned}&\left\{\left[\boldsymbol{J}^{-1}(\Theta)\right]_{\Theta_r\Theta_r}\right\}^{-1}\\&=\frac{1}{\sigma^2}\left[\|\boldsymbol{r}_t\|^2-\frac{\boldsymbol{r}_t^H\boldsymbol{r}_d\boldsymbol{r}_d^H\boldsymbol{r}_t}{\left(\|\boldsymbol{r}_d\|^2+\|\boldsymbol{r}_d'\|^2\right)}\right]\boldsymbol{I}_2\end{aligned} \tag{38}$$

The value of Θ_r under H_0 is

$$\Theta_{r0}=[0,0]^T \tag{39}$$

The MLE of Θ under H_1 is:

$$\begin{aligned}\hat{\beta}_1=&\left[\boldsymbol{r}_t^H\boldsymbol{z}-\boldsymbol{r}_t^H\boldsymbol{r}_d\left(\boldsymbol{r}_d^H\boldsymbol{z}+\boldsymbol{r}_d'^H\boldsymbol{z}'\right)\left(\boldsymbol{r}_d^H\boldsymbol{r}_d+\boldsymbol{r}_d'^H\boldsymbol{r}_d'\right)^{-1}\right]\\&\times\left[\|\boldsymbol{r}_t\|^2-\left|\boldsymbol{r}_d^H\boldsymbol{r}_t\right|^2\left(\boldsymbol{r}_d^H\boldsymbol{r}_d+\boldsymbol{r}_d'^H\boldsymbol{r}_d'\right)^{-1}\right]^{-1}\end{aligned} \tag{40}$$

$$\hat{\alpha}_1=\left(\boldsymbol{r}_d^H\boldsymbol{r}_d+\boldsymbol{r}_d'^H\boldsymbol{r}_d'\right)^{-1}\left(\boldsymbol{r}_d^H\boldsymbol{z}+\boldsymbol{r}_d'^H\boldsymbol{z}'-\hat{\beta}_1\boldsymbol{r}_d^H\boldsymbol{r}_t\right) \tag{41}$$

$$\hat{\sigma}_1^2=\frac{1}{N+K}\left\{\|\boldsymbol{z}\|^2+\|\boldsymbol{z}'\|^2-\frac{\left|\left(\boldsymbol{r}_d^H\boldsymbol{z}+\boldsymbol{r}_d'^H\boldsymbol{z}'\right)\right|^2}{\|\boldsymbol{r}_d\|^2+\|\boldsymbol{r}_d'\|^2}-\frac{\left|\boldsymbol{r}_t^H\left[\boldsymbol{z}-\frac{\boldsymbol{r}_d\left(\boldsymbol{r}_d^H\boldsymbol{z}+\boldsymbol{r}_d'^H\boldsymbol{z}'\right)}{\|\boldsymbol{r}_d\|^2+\|\boldsymbol{r}_d'\|^2}\right]\right|^2}{\left(\|\boldsymbol{r}_t\|^2-\frac{\boldsymbol{r}_d^H\boldsymbol{r}_t\boldsymbol{r}_t^H\boldsymbol{r}_d}{\|\boldsymbol{r}_d\|^2+\|\boldsymbol{r}_d'\|^2}\right)}\right\} \tag{42}$$

The complex-parameter Wald test with secondary data based on the FSR (referred to as Wald-SD-FSR) can be derived by substituting (38)–(42) into (37):

$$\begin{aligned}T_{Wald-SD-FSR}=&\left|\boldsymbol{r}_t^H\boldsymbol{z}-\frac{\boldsymbol{r}_t^H\boldsymbol{r}_d\left(\boldsymbol{r}_d^H\boldsymbol{z}+\boldsymbol{r}_d'^H\boldsymbol{z}'\right)}{\|\boldsymbol{r}_d\|^2+\|\boldsymbol{r}_d'\|^2}\right|^2\\&\times\left(\|\boldsymbol{r}_t\|^2-\frac{\left|\boldsymbol{r}_d^H\boldsymbol{r}_t\right|^2}{\|\boldsymbol{r}_d\|^2+\|\boldsymbol{r}_d'\|^2}\right)^{-1}\left[\|\boldsymbol{z}\|^2+\|\boldsymbol{z}'\|^2-\frac{\left|\left(\boldsymbol{r}_d^H\boldsymbol{z}+\boldsymbol{r}_d'^H\boldsymbol{z}'\right)\right|^2}{\|\boldsymbol{r}_d\|^2+\|\boldsymbol{r}_d'\|^2}\right.\\&\left.-\frac{\left|\boldsymbol{r}_t^H\left[\boldsymbol{z}-\frac{\boldsymbol{r}_d\left(\boldsymbol{r}_d^H\boldsymbol{z}+\boldsymbol{r}_d'^H\boldsymbol{z}'\right)}{\|\boldsymbol{r}_d\|^2+\|\boldsymbol{r}_d'\|^2}\right]\right|^2}{\left(\|\boldsymbol{r}_t\|^2-\frac{\boldsymbol{r}_d^H\boldsymbol{r}_t\boldsymbol{r}_t^H\boldsymbol{r}_d}{\|\boldsymbol{r}_d\|^2+\|\boldsymbol{r}_d'\|^2}\right)}\right]^{-1}\underset{H_0}{\overset{H_1}{\gtrless}}\eta'\end{aligned} \tag{43}$$

where η' denotes the modified detection threshold.

3. Design of Adaptive Detectors without Secondary Data

When the secondary data are not available, we formulate the detection problem as the following binary hypothesis test:

$$\begin{cases}H_0:\breve{\boldsymbol{z}}=\breve{\alpha}\,\breve{\boldsymbol{r}}_d+\breve{\boldsymbol{n}}\\H_1:\breve{\boldsymbol{z}}=\breve{\alpha}\,\breve{\boldsymbol{r}}_d+\breve{\beta}\,\breve{\boldsymbol{r}}_t+\breve{\boldsymbol{n}}\end{cases} \tag{44}$$

where $\breve{\boldsymbol{r}}_t \in \mathbb{C}_{N\times 1}$ and $\breve{\boldsymbol{r}}_d \in \mathbb{C}_{N\times 1}$ denote N -dimensional complex vectors containing samples collected from the target signal and direct signal, $\breve{\beta}$ and $\breve{\alpha}$ are unknown complex amplitudes of the target signal and direct signal, $\breve{\boldsymbol{z}} \in \mathbb{C}_{N\times 1}$ denotes the primary data, $\breve{\boldsymbol{n}}$ denotes the noise which satisfies $\breve{\boldsymbol{n}} \sim \mathcal{CN}\left(\boldsymbol{0}, \breve{\sigma}^2 \boldsymbol{I}_N\right)$, and $\breve{\sigma}^2$ denotes the noise variance.

The PDF of the primary data is

$$f\left(\breve{\boldsymbol{z}}|H_i\right) = \frac{1}{\pi^N \breve{\sigma}^{2N}} \exp\left[-\frac{1}{\breve{\sigma}^2}\left(\left\|\breve{\boldsymbol{z}} - \breve{\alpha}\breve{\boldsymbol{r}}_d - i\breve{\beta}\breve{\boldsymbol{r}}_t\right\|^2\right)\right] \tag{45}$$

where $i = 0,\ 1$.

3.1. Adaptive Complex Parameter Rao Detector without Secondary Data

The complex parameter Rao test without secondary data for the detection problem (44) is

$$\left.\frac{\partial \ln f\left(\breve{\boldsymbol{z}}|H_1\right)}{\partial \breve{\Theta}_r}\right|^T_{\breve{\Theta}=\hat{\breve{\Theta}}_0} \left[\boldsymbol{J}^{-1}\left(\hat{\breve{\Theta}}_0\right)\right]_{\breve{\Theta}_r\breve{\Theta}_r} \left.\frac{\partial \ln f\left(\breve{\boldsymbol{z}}|H_1\right)}{\partial \breve{\Theta}_r^*}\right|_{\breve{\Theta}=\hat{\breve{\Theta}}_0} \underset{H_0}{\overset{H_1}{\gtrless}} \varepsilon \tag{46}$$

where $\breve{\Theta}_r = \left[\breve{\beta}^T, \breve{\beta}^H\right]^T$, $\breve{\Theta}_s = \left[\breve{\alpha}^T, \breve{\alpha}^H, \breve{\sigma}^2\right]^T$, $\hat{\breve{\Theta}}_0$ is the MLE of $\breve{\Theta}$ under H_0, and ε denotes the detection threshold.

According to the PDF of the primary data and the theory of complex-valued matrix differentiation [40], we can obtain the following results:

$$\frac{\partial \ln f\left(\breve{\boldsymbol{z}}|H_1\right)}{\partial \breve{\beta}^*} = \frac{1}{\breve{\sigma}^2}\left(\breve{\boldsymbol{r}}_t^H \breve{\boldsymbol{z}} - \breve{\alpha}\breve{\boldsymbol{r}}_t^H \breve{\boldsymbol{r}}_d - \breve{\beta}\breve{\boldsymbol{r}}_t^H \breve{\boldsymbol{r}}_t\right) \tag{47}$$

$$\frac{\partial \ln f\left(\breve{\boldsymbol{z}}|H_1\right)}{\partial \breve{\beta}} = \frac{1}{\breve{\sigma}^2}\left(\breve{\boldsymbol{z}}^H \breve{\boldsymbol{r}}_t - \breve{\alpha}^H\breve{\boldsymbol{r}}_d^H \breve{\boldsymbol{r}}_t - \breve{\beta}^H\breve{\boldsymbol{r}}_t^H \breve{\boldsymbol{r}}_t\right) \tag{48}$$

The FIM $\boldsymbol{J}\left(\breve{\Theta}\right)$ when the secondary data are not available is calculated in a similar way as the FIM $\boldsymbol{J}(\Theta)$ when the secondary data are available. After some calculation, the four blocks of $\boldsymbol{J}\left(\breve{\Theta}\right)$ are

$$\boldsymbol{J}_{\breve{\Theta}_r\breve{\Theta}_r} = \frac{1}{\breve{\sigma}^2}\begin{bmatrix} \breve{\boldsymbol{r}}_t^H \breve{\boldsymbol{r}}_t & 0 \\ 0 & \breve{\boldsymbol{r}}_t^H \breve{\boldsymbol{r}}_t \end{bmatrix} \tag{49}$$

$$\boldsymbol{J}_{\breve{\Theta}_r\breve{\Theta}_s} = \frac{1}{\breve{\sigma}^2}\begin{bmatrix} \breve{\boldsymbol{r}}_t^H \breve{\boldsymbol{r}}_d & 0 & 0 \\ 0 & \breve{\boldsymbol{r}}_d^H \breve{\boldsymbol{r}}_t & 0 \end{bmatrix} \tag{50}$$

$$\boldsymbol{J}_{\breve{\Theta}_s\breve{\Theta}_s} = \frac{1}{\breve{\sigma}^2}\begin{bmatrix} \breve{\boldsymbol{r}}_d^H \breve{\boldsymbol{r}}_d & 0 & 0 \\ 0 & \breve{\boldsymbol{r}}_d^H \breve{\boldsymbol{r}}_d & 0 \\ 0 & 0 & \frac{N}{\breve{\sigma}^2} \end{bmatrix} \tag{51}$$

$$\left\{\left[\boldsymbol{J}^{-1}\left(\breve{\Theta}\right)\right]_{\breve{\Theta}_r\breve{\Theta}_r}\right\}^{-1} = \frac{1}{\breve{\sigma}^2}\begin{bmatrix} \left\|\breve{\boldsymbol{r}}_t\right\|^2 - \frac{\left|\breve{\boldsymbol{r}}_d^H \breve{\boldsymbol{r}}_t\right|^2}{\left\|\breve{\boldsymbol{r}}_d\right\|^2} & 0 \\ 0 & \left\|\breve{\boldsymbol{r}}_t\right\|^2 - \frac{\left|\breve{\boldsymbol{r}}_d^H \breve{\boldsymbol{r}}_t\right|^2}{\left\|\breve{\boldsymbol{r}}_d\right\|^2} \end{bmatrix} \tag{52}$$

The MLEs of the unknown parameters under H_0 are: $\hat{\breve{\sigma}}_0^2 = \left(\left\| \breve{\boldsymbol{z}} \right\|^2 - \frac{\left| \breve{\boldsymbol{r}}_d^H \breve{\boldsymbol{z}} \right|^2}{\left\| \breve{\boldsymbol{r}}_d \right\|^2} \right) / N$, $\hat{\breve{\beta}}_0 = 0$, and $\hat{\breve{\alpha}}_0 = \left(\breve{\boldsymbol{r}}_d^H \breve{\boldsymbol{r}}_d \right)^{-1} \left(\breve{\boldsymbol{r}}_d^H \breve{\boldsymbol{z}} \right)$.

Substituting (47)–(52) and the MLEs of the unknown parameters under H_0 into (46), we have the complex parameter Rao test without secondary data based on the forward scatter radar (referred to as Rao-FSR):

$$T_{Rao-FSR} = \frac{2}{\hat{\breve{\sigma}}_0^2} \left| \breve{\boldsymbol{r}}_t^H \left(\breve{\boldsymbol{z}} - \frac{\breve{\boldsymbol{r}}_d \breve{\boldsymbol{r}}_d^H \breve{\boldsymbol{z}}}{\left\| \breve{\boldsymbol{r}}_d \right\|^2} \right) \right|^2 \left(\left\| \breve{\boldsymbol{r}}_t \right\|^2 - \frac{\breve{\boldsymbol{r}}_t^H \breve{\boldsymbol{r}}_d \breve{\boldsymbol{r}}_d^H \breve{\boldsymbol{r}}_t}{\left\| \breve{\boldsymbol{r}}_d \right\|^2} \right)^{-1} \underset{H_0}{\overset{H_1}{\gtrless}} \varepsilon \tag{53}$$

3.2. Adaptive Complex Parameter Wald Detector without Secondary Data

The complex parameter Wald test without secondary data is given by

$$\left(\hat{\breve{\Theta}}_{r1} - \breve{\Theta}_{r0} \right)^H \left\{ \left[\boldsymbol{J}^{-1} \left(\hat{\breve{\Theta}}_1 \right) \right]_{\breve{\Theta}_r \breve{\Theta}_r} \right\}^{-1} \left(\hat{\breve{\Theta}}_{r1} - \breve{\Theta}_{r0} \right) \underset{H_0}{\overset{H_1}{\gtrless}} \rho \tag{54}$$

where ρ denotes the detection threshold, $\hat{\breve{\Theta}}_1$ and $\hat{\breve{\Theta}}_{r1}$ are the MLEs of $\breve{\Theta}$ and $\breve{\Theta}_r$ under H_1, and $\breve{\Theta}_{r0}$ is the value of $\breve{\Theta}_r$ under H_0, $\breve{\Theta}_{r0} = [0, 0]^T$.

The second term of the Wald test is obtained according to the four blocks of $\boldsymbol{J}\left(\breve{\Theta} \right)$, namely, (49)–(51) and the MLEs of unknown parameters under H_1: $\hat{\breve{\alpha}}_1 = \left(\breve{\boldsymbol{r}}_d^H \breve{\boldsymbol{r}}_d \right)^{-1} \left(\breve{\boldsymbol{r}}_d^H \boldsymbol{z} - \hat{\breve{\beta}}_1 \breve{\boldsymbol{r}}_d^H \breve{\boldsymbol{r}}_t \right)$, $\hat{\breve{\beta}}_1 = \widetilde{\boldsymbol{r}}_t^H \widetilde{\boldsymbol{z}} / \left\| \widetilde{\boldsymbol{r}}_t \right\|^2$, and $\hat{\breve{\sigma}}_1^2 = \left\| \boldsymbol{P}_{\widetilde{\boldsymbol{r}}_t}^{\perp} \widetilde{\boldsymbol{z}} \right\|^2 / N$:

$$\left\{ \left[\boldsymbol{J}^{-1} \left(\hat{\breve{\Theta}}_1 \right) \right]_{\breve{\Theta}_r \breve{\Theta}_r} \right\}^{-1} = \frac{N}{\left\| \boldsymbol{P}_{\widetilde{\boldsymbol{r}}_t}^{\perp} \widetilde{\boldsymbol{z}} \right\|^2} \left(\left\| \breve{\boldsymbol{r}}_t \right\|^2 - \frac{\left| \breve{\boldsymbol{r}}_d^H \breve{\boldsymbol{r}}_t \right|^2}{\left\| \breve{\boldsymbol{r}}_d \right\|^2} \right) \boldsymbol{I}_2 \tag{55}$$

where $\boldsymbol{P}_{rd}^{\perp} = \boldsymbol{I}_N - \frac{\breve{\boldsymbol{r}}_d \breve{\boldsymbol{r}}_d^H}{\left\| \breve{\boldsymbol{r}}_d \right\|^2}$, $\widetilde{\boldsymbol{r}}_t = \boldsymbol{P}_{rd}^{\perp} \breve{\boldsymbol{r}}_t$, $\widetilde{\boldsymbol{z}} = \boldsymbol{P}_{rd}^{\perp} \breve{\boldsymbol{z}}$, $\boldsymbol{P}_{\widetilde{\boldsymbol{r}}_t} = \widetilde{\boldsymbol{r}}_t \left(\widetilde{\boldsymbol{r}}_t^H \widetilde{\boldsymbol{r}}_t \right)^{-1} \widetilde{\boldsymbol{r}}_t^H$, $\boldsymbol{P}_{\widetilde{\boldsymbol{r}}_t}^{\perp} = \boldsymbol{I}_N - \boldsymbol{P}_{\widetilde{\boldsymbol{r}}_t}$.

Plugging (55) and the MLEs of the unknown parameters under H_1 into (54), we have the complex parameter Wald test without secondary data based on the FSR (referred to as Wald-FSR):

$$T_{Wald-FSR} = 2N \left\| \boldsymbol{P}_{\widetilde{\boldsymbol{r}}_t} \widetilde{\boldsymbol{z}} \right\|^2 / \left\| \boldsymbol{P}_{\widetilde{\boldsymbol{r}}_t}^{\perp} \widetilde{\boldsymbol{z}} \right\|^2 \underset{H_0}{\overset{H_1}{\gtrless}} \rho \tag{56}$$

4. The Equivalence of the Wald Test, Rao Test, and GLRT

4.1. The Equivalence of the Wald Test, Rao Test, and GLRT with Secondary Data

In this part, the equivalence of the Wald test, Rao test, and GLRT is validated when the secondary data are available. We rewrite the test statistics of the Rao-SD-FSR (36) and the Wald-SD-FSR (43) as

$$
\begin{aligned}
T_{Rao-SD-FSR} = {} & \frac{\left| \boldsymbol{r}_t^H \left[\boldsymbol{z} - \frac{\boldsymbol{r}_d\left(\boldsymbol{r}_d^H \boldsymbol{z} + \boldsymbol{r}_d'^H \boldsymbol{z}'\right)}{\|\boldsymbol{r}_d\|^2 + \|\boldsymbol{r}_d'\|^2} \right] \right|^2 \left(\|\boldsymbol{r}_t\|^2 - \frac{\boldsymbol{r}_d^H \boldsymbol{r}_t \boldsymbol{r}_t^H \boldsymbol{r}_d}{\|\boldsymbol{r}_d\|^2 + \|\boldsymbol{r}_d'\|^2} \right)^{-1}}{\|\boldsymbol{z}\|^2 + \|\boldsymbol{z}'\|^2 - \frac{\left|\left(\boldsymbol{r}_d^H \boldsymbol{z} + \boldsymbol{r}_d'^H \boldsymbol{z}'\right)\right|^2}{\|\boldsymbol{r}_d\|^2 + \|\boldsymbol{r}_d'\|^2}} \\
& - \frac{\left[\|\boldsymbol{z}\|^2 + \|\boldsymbol{z}'\|^2 - \frac{\left|\left(\boldsymbol{r}_d^H \boldsymbol{z} + \boldsymbol{r}_d'^H \boldsymbol{z}'\right)\right|^2}{\|\boldsymbol{r}_d\|^2 + \|\boldsymbol{r}_d'\|^2} \right]}{\|\boldsymbol{z}\|^2 + \|\boldsymbol{z}'\|^2 - \frac{\left|\left(\boldsymbol{r}_d^H \boldsymbol{z} + \boldsymbol{r}_d'^H \boldsymbol{z}'\right)\right|^2}{\|\boldsymbol{r}_d\|^2 + \|\boldsymbol{r}_d'\|^2}} + 1 \\
= {} & 1 - \left\{ \left[\|\boldsymbol{z}\|^2 + \|\boldsymbol{z}'\|^2 - \frac{\left|\left(\boldsymbol{r}_d^H \boldsymbol{z} + \boldsymbol{r}_d'^H \boldsymbol{z}'\right)\right|^2}{\|\boldsymbol{r}_d\|^2 + \|\boldsymbol{r}_d'\|^2} \right] \left[\|\boldsymbol{z}\|^2 + \|\boldsymbol{z}'\|^2 \right.\right. \\
& \left.\left. - \frac{\left|\left(\boldsymbol{r}_d^H \boldsymbol{z} + \boldsymbol{r}_d'^H \boldsymbol{z}'\right)\right|^2}{\|\boldsymbol{r}_d\|^2 + \|\boldsymbol{r}_d'\|^2} - \frac{\left| \boldsymbol{r}_t^H \left[\boldsymbol{z} - \frac{\boldsymbol{r}_d\left(\boldsymbol{r}_d^H \boldsymbol{z} + \boldsymbol{r}_d'^H \boldsymbol{z}'\right)}{\|\boldsymbol{r}_d\|^2 + \|\boldsymbol{r}_d'\|^2} \right] \right|^2}{\left(\|\boldsymbol{r}_t\|^2 - \frac{\boldsymbol{r}_d^H \boldsymbol{r}_t \boldsymbol{r}_t^H \boldsymbol{r}_d}{\|\boldsymbol{r}_d\|^2 + \|\boldsymbol{r}_d'\|^2} \right)} \right]^{-1} \right\}^{-1} \\
= {} & 1 - \left[\frac{T_{GLRT-SD-FSR}}{(N+K-2)} + 1 \right]^{-1}
\end{aligned} \tag{57}
$$

$$
\begin{aligned}
& T_{Wald-SD-FSR} \\
& = \left| \boldsymbol{r}_t^H \boldsymbol{z} - \frac{\boldsymbol{r}_t^H \boldsymbol{r}_d\left(\boldsymbol{r}_d^H \boldsymbol{z} + \boldsymbol{r}_d'^H \boldsymbol{z}'\right)}{\|\boldsymbol{r}_d\|^2 + \|\boldsymbol{r}_d'\|^2} \right|^2 \left(\|\boldsymbol{r}_t\|^2 - \frac{\left|\boldsymbol{r}_d^H \boldsymbol{r}_t\right|^2}{\|\boldsymbol{r}_d\|^2 + \|\boldsymbol{r}_d'\|^2} \right)^{-1} \\
& \times \left[\|\boldsymbol{z}\|^2 + \|\boldsymbol{z}'\|^2 - \frac{\left|\left(\boldsymbol{r}_d^H \boldsymbol{z} + \boldsymbol{r}_d'^H \boldsymbol{z}'\right)\right|^2}{\|\boldsymbol{r}_d\|^2 + \|\boldsymbol{r}_d'\|^2} - \frac{\left| \boldsymbol{r}_t^H \left[\boldsymbol{z} - \frac{\boldsymbol{r}_d\left(\boldsymbol{r}_d^H \boldsymbol{z} + \boldsymbol{r}_d'^H \boldsymbol{z}'\right)}{\|\boldsymbol{r}_d\|^2 + \|\boldsymbol{r}_d'\|^2} \right] \right|^2}{\left(\|\boldsymbol{r}_t\|^2 - \frac{\boldsymbol{r}_d^H \boldsymbol{r}_t \boldsymbol{r}_t^H \boldsymbol{r}_d}{\|\boldsymbol{r}_d\|^2 + \|\boldsymbol{r}_d'\|^2} \right)} \right]^{-1} \\
& = \frac{T_{GLRT-SD-FSR}}{(N+K-2)}
\end{aligned} \tag{58}
$$

where $T_{GLRT-SD-FSR} = (N+K-2)\Omega\Xi^{-1}\left(\Gamma - \Omega\Xi^{-1}\right)^{-1}$ is the GLRT with secondary data based on the FSR (referred to as GLRT-SD-FSR) [22], $\Xi = \|\boldsymbol{r}_t\|^2 - \frac{\left|\boldsymbol{r}_d^H \boldsymbol{r}_t\right|^2}{\|\boldsymbol{r}_d\|^2 + \|\boldsymbol{r}_d'\|^2}$, $\Omega = \left| \boldsymbol{r}_t^H \boldsymbol{z} - \frac{\boldsymbol{r}_t^H \boldsymbol{r}_d\left(\boldsymbol{r}_d^H \boldsymbol{z} + \boldsymbol{r}_d'^H \boldsymbol{z}'\right)}{\|\boldsymbol{r}_d\|^2 + \|\boldsymbol{r}_d'\|^2} \right|^2$, and $\Gamma = \|\boldsymbol{z}\|^2 + \|\boldsymbol{z}'\|^2 - \frac{\left|\left(\boldsymbol{r}_d^H \boldsymbol{z} + \boldsymbol{r}_d'^H \boldsymbol{z}'\right)\right|^2}{\|\boldsymbol{r}_d\|^2 + \|\boldsymbol{r}_d'\|^2}$. Equations (57) and (58) show that the Wald test and Rao test are proportional to the GLRT, namely, the three detectors coincide for adaptive moving rectangular-shaped target detection in FSR when the secondary data are available.

4.2. The Equivalence of the Wald Test, Rao Test, and GLRT without Secondary Data

The equivalence of the Wald test, Rao test and GLRT when the secondary data are not available is validated in this part. The test statistics of the Rao-FSR (53) and Wald-FSR (56) can be rewritten as:

$$
\begin{aligned}
T_{Rao-FSR} &= 2N\left|\breve{\boldsymbol{r}}_t^H\left(\breve{\boldsymbol{z}}-\frac{\boldsymbol{r}'_d\boldsymbol{r}'^H_d\breve{\boldsymbol{z}}}{\left\|\breve{\boldsymbol{r}}_d\right\|^2}\right)\right|^2 \\
&\times\left[\left(\left\|\breve{\boldsymbol{r}}_t\right\|^2-\frac{\breve{\boldsymbol{r}}_t^H\breve{\boldsymbol{r}}_d\breve{\boldsymbol{r}}_d^H\breve{\boldsymbol{r}}_t}{\left\|\breve{\boldsymbol{r}}_d\right\|^2}\right)\left(\left\|\breve{\boldsymbol{z}}\right\|^2-\frac{\left|\breve{\boldsymbol{r}}_d^H\breve{\boldsymbol{z}}\right|^2}{\left\|\breve{\boldsymbol{r}}_d\right\|^2}\right)\right]^{-1} \\
&= 2N\left|\breve{\boldsymbol{r}}_t^H\boldsymbol{P}_{rd}^{\perp}\breve{\boldsymbol{z}}\right|^2/\left[\left(\breve{\boldsymbol{r}}_t^H\boldsymbol{P}_{rd}^{\perp}\breve{\boldsymbol{r}}_t\right)\left(\breve{\boldsymbol{z}}^H\boldsymbol{P}_{rd}^{\perp}\breve{\boldsymbol{z}}\right)\right] \\
&= 2N\left|\tilde{\boldsymbol{r}}_t^H\tilde{\boldsymbol{z}}\right|^2/\left[\left(\tilde{\boldsymbol{r}}_t^H\tilde{\boldsymbol{r}}_t\right)\left(\tilde{\boldsymbol{z}}^H\tilde{\boldsymbol{z}}\right)\right] \\
&= 2N\tilde{\boldsymbol{z}}^H\boldsymbol{P}_{\tilde{\boldsymbol{r}}_t}\tilde{\boldsymbol{z}}/\left(\tilde{\boldsymbol{z}}^H\boldsymbol{P}_{\tilde{\boldsymbol{r}}_t}^{\perp}\tilde{\boldsymbol{z}}+\tilde{\boldsymbol{z}}^H\boldsymbol{P}_{\tilde{\boldsymbol{r}}_t}\tilde{\boldsymbol{z}}\right) \\
&= \frac{2N\left\|\boldsymbol{P}_{\tilde{\boldsymbol{r}}_t}\tilde{\boldsymbol{z}}\right\|^2/\left\|\boldsymbol{P}_{\tilde{\boldsymbol{r}}_t}^{\perp}\tilde{\boldsymbol{z}}\right\|^2}{1+\left\|\boldsymbol{P}_{\tilde{\boldsymbol{r}}_t}\tilde{\boldsymbol{z}}\right\|^2/\left\|\boldsymbol{P}_{\tilde{\boldsymbol{r}}_t}^{\perp}\tilde{\boldsymbol{z}}\right\|^2} = \frac{2NT_{GLRT-FSR}/(N-2)}{1+T_{GLRT-FSR}/(N-2)}
\end{aligned}
\tag{59}
$$

$$
T_{Wald-FSR} = 2N\left\|\boldsymbol{P}_{\tilde{\boldsymbol{r}}_t}\tilde{\boldsymbol{z}}\right\|^2/\left\|\boldsymbol{P}_{\tilde{\boldsymbol{r}}_t}^{\perp}\tilde{\boldsymbol{z}}\right\|^2 = 2NT_{GLRT-FSR}/(N-2)
\tag{60}
$$

where $T_{GLRT-FSR} = (N-2)\left\|\boldsymbol{P}_{\tilde{\boldsymbol{r}}_t}\tilde{\boldsymbol{z}}\right\|^2/\left\|\boldsymbol{P}_{\tilde{\boldsymbol{r}}_t}^{\perp}\tilde{\boldsymbol{z}}\right\|^2$ is the GLRT without secondary data based on the FSR (referred to as GLRT-FSR) [22]. Equations (59) and (60) indicate that the GLRT and the complex parameter Rao and Wald detectors are identical for adaptive target detection in complex white Gaussian noise using the FSR when the secondary data are not available.

For the problem of adaptive detection of a signal using the monostatic radar in a homogeneous environment wherein the primary data and the secondary data share the same noise covariance matrix, the GLRT, Wald and Rao detectors are demonstrated to be three different detectors [41–43]. For cases involving partially homogeneous environment wherein the primary data and the secondary data have different noise variance, the GLRT, Wald, and Rao tests coincide [44]. Different from monostatic radar, Equations (57)–(60) indicate that the three tests for FSR coincide with each other in the complex white Gaussian noise wherein the primary data and the secondary data have equal variance. A possible reason for the difference is that the noise follows the complex white Gaussian distribution for the problem of adaptive moving target detection using the FSR.

5. Numerical Evaluation

Monte Carlo simulations were conducted to assess the detection performance of the proposed Rao-SD-FSR, Wald-SD-FSR, Rao-FSR, and Wald-FSR detectors in this section. For comparison, the simulation results of the GLRT-SD-FSR, the GLRT-FSR, the CVD [21], and the ideal optimum detector [22] derived by assuming that both the direct signal and the noise parameters are known are also given. All the simulations are carried out using the Matlab (R2020b).

When the far-field parameter $f_f = 2(\max\{L_h, L_v\})^2/\lambda(\min\{R_0, R-R_0\})$ is smaller than 1, the target is in the far field of both the transmitter and receiver, and vice versa, the target is in the near field. Two cases are considered: the target is in the far field of the receiver and the transmitter ($R = 4000$), and the target approaches the near field but is still in the far field ($R = 600$). The direct signal-to-noise spectral density power ratio (DNSR) is [21]: $\text{DNSR} = \frac{|\alpha|^2}{N_0}$, where $N_0 = BT_eF$ denotes a one-sided noise spectral density, F denotes the noise figure, T_e denotes the standard temperature, and B denotes Boltzmann's constant. The target parameters and radar system parameters of the two cases are given in Table 1.

Table 1. The target parameters and radar system parameters.

Parameters	Symbol	Value
Carrier Frequency	f_c	2.4 GHz
Horizontal Dimension	L_h	4 m
Vertical Dimension	L_v	1 m
Target Velocity	v	25 m/s
Base Line	R	4000 m, 600 m
Distance	R_0	$R/2$

5.1. Performance Analysis of the Proposed Detectors with Secondary Data

In this part, the detection performance of the proposed Rao-SD-FSR and Wald-SD-FSR was analyzed when the secondary data are available. In Figure 2, the probability of detection P_d is plotted as a function of the DNSR. The probabilities of detection of the proposed Rao-SD-FSR and Wald-SD-FSR are obtained from the test statistics (36) and (43). For comparison, the simulated and theoretical probabilities of detection of the GLRT-SD-FSR and the ideal optimum detector are also given.

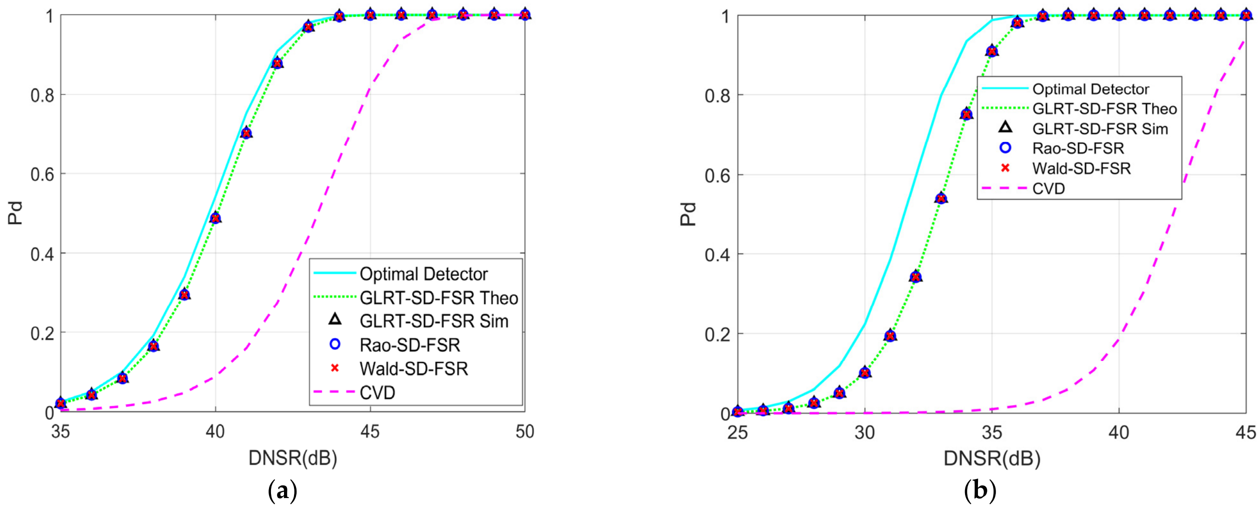

Figure 2. Probability of detection versus DNSR (**a**) $R = 4000, K = N$ (**b**) $R = 600, K = N$.

We can see that the proposed Rao-SD-FSR and Wald-SD-FSR detectors and the GLRT-SD-FSR coincide with each other. Moreover, simulation results of the three detectors are all in agreement with the theoretical result of the GLRT-SD-FSR. Thus, both simulation results and the theoretical analysis demonstrate the equivalence of the complex parameter Wald detector, complex Rao detector, and the GLRT detector for the detection problem (1).

From Figure 2, we can also see that the probabilities of detection of all the detectors improve as the DNSR increases. Meanwhile, the proposed Rao-SD-FSR and Wald-SD-FSR outperform the CVD. The detection performance gains of the Rao-SD-FSR and Wald-SD-FSR with respect to the CVD are about 3 dB and 10 dB for $P_d = 0.9, R = 4000$ and $P_d = 0.9, R = 600$. Moreover, the proposed Rao-SD-FSR and Wald-SD-FSR detectors achieve similar detection performance to the ideal optimum detector. The performance losses of the Rao-SD-FSR and Wald-SD-FSR detectors compared with the ideal optimum GLRT are about 0.5 dB and 1 dB for $P_d = 0.9$, $R = 4000$ and $P_d = 0.9, R = 600$. When comparing Figure 2a with Figure 2b, it can be seen that the detection performance degradation of the proposed Rao-SD-FSR and Wald-SD-FSR with respect to the ideal optimum detector when the target approaches the near field is higher than those when the target is in the far field.

The receiver operating characteristic (ROC) curve, which is plotted with the probability of false alarm P_{fa} as the horizontal coordinate and the probability of detection P_d as the vertical coordinate, is a widely used evaluation tool for signal detection. To see the impact of the observation time T on the performance of the Rao-SD-FSR and Wald-SD-FSR, the receiver operating characteristic (ROC) of the Rao-SD-FSR and Wald-SD-FSR is plotted for different observation times when $R = 4000$, $DNSR = 35$ dB and $R = 600$, $DNSR = 30$ dB in Figure 3a,b. Figure 3 indicates that the detection performance of the proposed detectors improves with an increase in the observation time and approaches that of the ideal optimum detector when the long observation time is used. Thus, the increase in the observation time can achieve a detection performance gain.

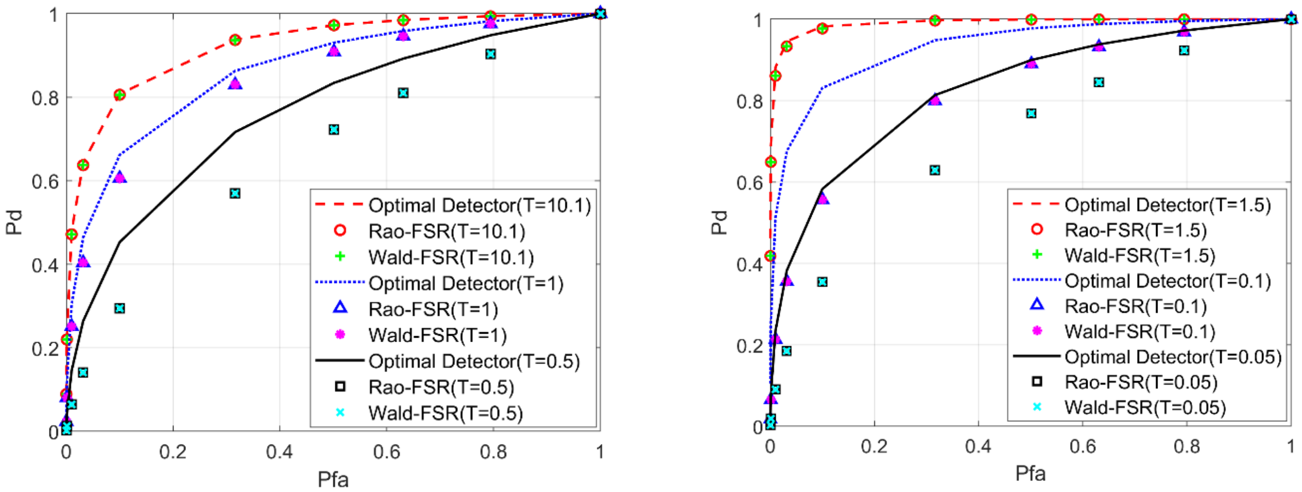

(**a**) (**b**)

Figure 3. ROC of the detectors (**a**) $R = 4000$, $DSNR = 35$ dB; (**b**) $R = 600$, $DSNR = 30$ dB.

In Figure 4, probabilities of detection of the Rao-SD-FSR and Wald-SD-FSR are plotted as a function of the number of the secondary data K. We can see that the probabilities of detection of the Rao-SD-FSR and Wald-SD-FSR become higher when the number of the secondary data increases. This is due to the fact that the estimations of the unknown parameters become more accurate as the secondary data increase.

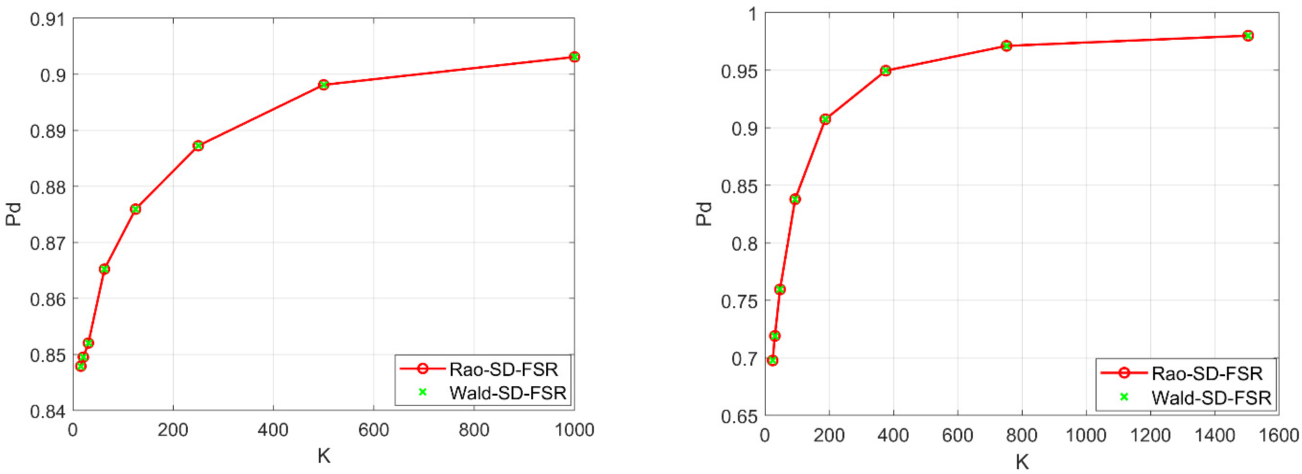

(**a**) (**b**)

Figure 4. Probability of detection versus K (**a**) $R = 4000$, $DSNR = 42$ dB; (**b**) $R = 600$, $DSNR = 35$ dB.

5.2. Performance Analysis of the Proposed Detectors without Secondary Data

In this part, the detection performance of the Rao-FSR and Wald-FSR detectors when the secondary data are not available is analyzed.

Figure 5 shows P_d versus DNSR for $R = 4000$ and $R = 600$. The probabilities of detection of the Rao-FSR and Wald-FSR are obtained by the test statistics (53) and (56). For comparison, probabilities of detection of the GLRT-FSR and the proposed Rao-SD-FSR and Wald-SD-FSR detectors are also given. From Figure 5, we can see that the Rao-FSR, GLRT-FSR, and Wald-FSR detectors coincide, which is consistent with the theoretical analysis. Meanwhile, the Rao-FSR and Wald-FSR detectors achieve about 3 dB and 8 dB detection performance improvement with respect to the CVD. Compared with the proposed Rao-SD-FSR and Wald-SD-FSR, the Rao-FSR and Wald-FSR detectors suffer detection performance degradation if the secondary data are not available. The detection performance losses are about 0.5 dB and 1.5 dB for $P_d = 0.9, R = 4000$ and $P_d = 0.9, R = 600$.

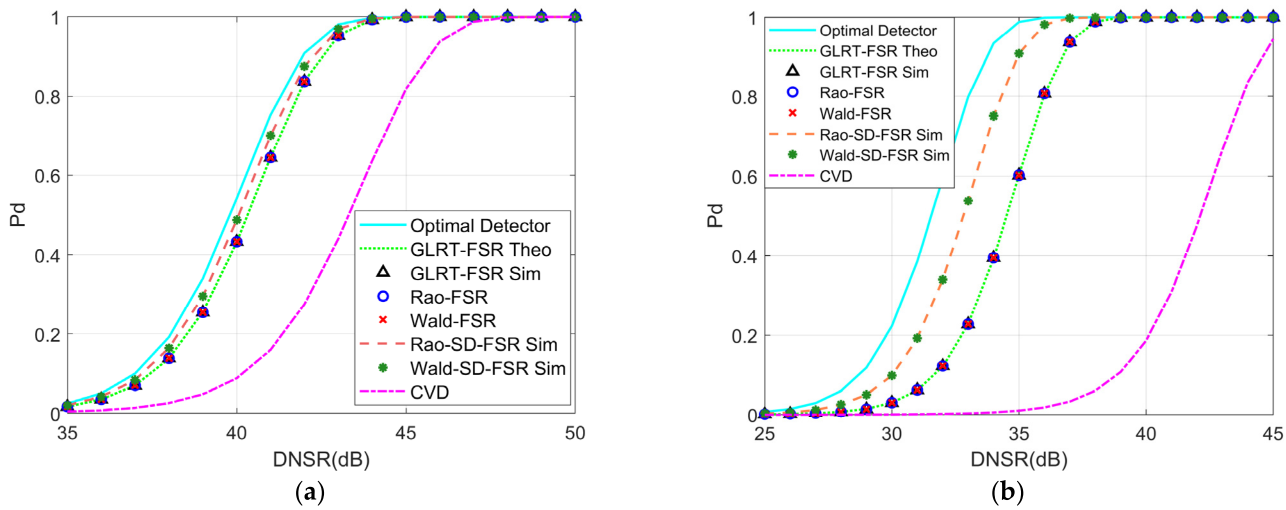

Figure 5. Probability of detection versus DNSR: (**a**) $R = 4000$; (**b**) $R = 600$.

In Figure 6, the impact of the observation time on the performance of the Rao-FSR and Wald-FSR detectors is analyzed. Figure 6 shows that the probabilities of detection of the Rao-FSR and Wald-FSR detectors approach the ideal optimum detector as the observation time increases. The impact of the observation time on the detection performance of the Rao-FSR and Wald-FSR is in agreement with the proposed Rao-SD-FSR and Wald-SD-FSR.

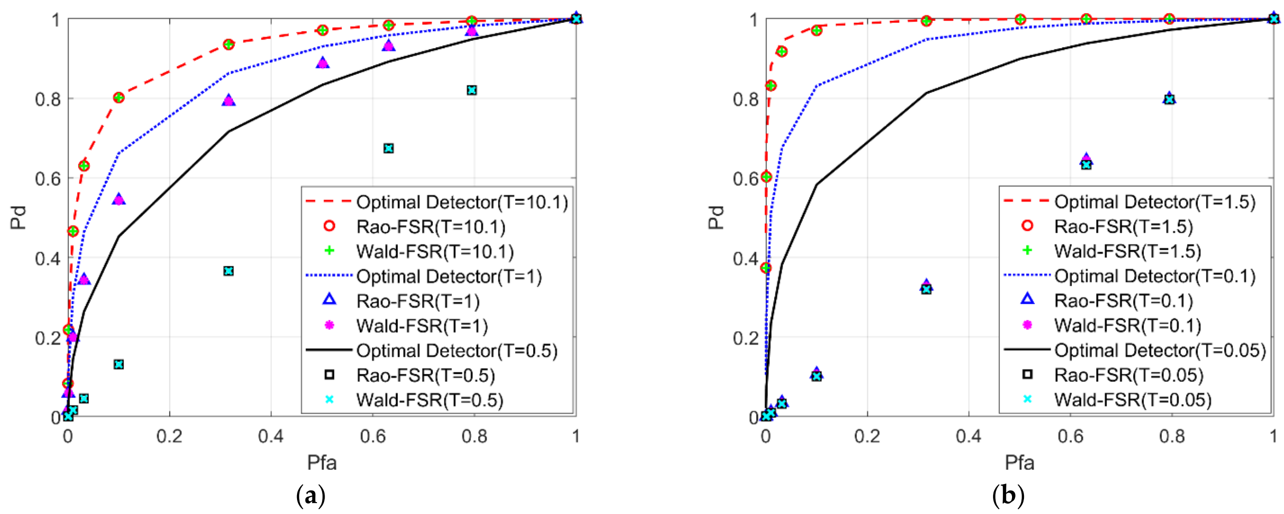

Figure 6. ROC of the detectors: (**a**) $R = 4000, DSNR = 35$ dB; (**b**) $R = 600, DSNR = 30$ dB.

6. Conclusions

In this paper, adaptive moving rectangular-shaped target detection in complex Gaussian noise using FSR has been discussed. Adaptive complex parameter Rao detectors and adaptive complex parameter Wald detectors, which regard the complex parameter as a whole, were designed when the secondary data were available and not available. The equivalence of the proposed complex parameter Rao and Wald tests to the GLRT has been verified by both the theoretical analysis and the simulation results. Meanwhile, the performance assessment shows that the proposed Rao-FSR, Rao-SD-FSR, Wald-FSR, and Wald-SD-FSR outperform the CVD and can achieve detection performance gains with the increase in the observation time and the number of the secondary data.

Author Contributions: Conceptualization, Z.W., D.W. and H.C.; methodology, Z.W. and H.C.; software, Z.W. and Y.L.; validation, Y.L., H.C. and D.W.; formal analysis, H.C.; investigation, Z.W. and Y.L.; resources, Z.W.; data curation, Z.W. and H.C.; writing—original draft preparation, Z.W. and D.W.; writing—review and editing, H.C. and Y.L.; visualization, Y.L.; supervision, D.W.; project administration, D.W. and H.C.; funding acquisition, Z.W. and Y.L. All authors have read and agreed to the published version of the manuscript.

Funding: This research was funded by National Natural Science Foundation of China, grant number 62301073 and 62171337, Foundation of National Key Laboratory of Radar Signal Processing, grant number JKW202301, National Key R&D Program of China, grant number 2018YFB2202500.

Data Availability Statement: Data are contained within the article.

Acknowledgments: The authors would like to thank the anonymous reviewers and the associate editor for their valuable comments.

Conflicts of Interest: The authors declare no conflicts of interest.

References

1. Mertens, M.; Koch, W.; Kirubarajan, T. Exploiting Doppler Blind Zone Information for Ground Moving Target Tracking with Bistatic Airborne Radar. *IEEE Trans. Aerosp. Electron. Syst.* **2014**, *50*, 130–148. [CrossRef]
2. Sun, H. Conceptual Study on Bistatic Shipborne High Frequency Surface Wave Radar. *IEEE Trans. Aerosp. Electron. Syst. Mag.* **2018**, *33*, 4–13. [CrossRef]
3. Zhang, J.; Ding, T.; Zhang, L. Longtime Coherent Integration Algorithm for High-Speed Maneuvering Target Detection Using Space-Based Bistatic Radar. *IEEE Trans. Geosci. Remote Sens.* **2022**, *60*, 5100216. [CrossRef]
4. Vu, V.T.; Pettersson, M.I. Nyquist Sampling Requirements for Polar Grids in Bistatic Time-Domain Algorithms. *IEEE Trans. Signal Process.* **2015**, *63*, 457–465. [CrossRef]
5. Boyle, R.J.; Wasylkiwskyj, W. Comparison of Monostatic and Bistatic Bearing Estimation Performance for Low RCS Targets. *IEEE Trans. Aerosp. Electron. Syst.* **1994**, *30*, 962–968. [CrossRef]
6. Falconi, M.T.; Lombardo, P.; Pastina, D.; Marzano, F.S. A Closed-Form Model for Long- and Short-Range Forward Scatter Radar Signals from Rectangular Conductive Targets. *IEEE Trans. Aerosp. Electron. Syst.* **2020**, *56*, 1370–1390. [CrossRef]
7. Suberviola, I.; Mayordomo, I.; Mendizabal, J. Experimental Results of Air Target Detection with a GPS Forward-Scattering Radar. *IEEE Geosci. Remote Sens. Lett.* **2012**, *9*, 47–51. [CrossRef]
8. Pairon, T.; Craeye, C.; Oestges, C. Improved Physical Optics Computation Near the Forward Scattering Region: Application to 2-D Scenarios. *IEEE Trans. Antennas Propag.* **2021**, *69*, 417–428. [CrossRef]
9. Clemente, C.; Soraghan, J.J. GNSS-Based Passive Bistatic Radar for Micro-Doppler Analysis of Helicopter Rotor Blades. *IEEE Trans. Aerosp. Electron. Syst.* **2014**, *50*, 491–500. [CrossRef]
10. Garvanov, I.; Kabakchiev, C.; Behar, V.; Daskalov, P. Air target detection with a GPS forward-scattering radar. In Proceedings of the 2016 19th International Symposium on Electrical Apparatus and Technologies (SIELA), Bourgas, Bulgaria, 29 May–1 June 2016.
11. Ustalli, N.; Pastina, D.; Lombardo, P. Target Motion Parameters Estimation in Forward Scatter Radar. *IEEE Trans. Aerosp. Electron. Syst.* **2020**, *56*, 226–248. [CrossRef]
12. Ai, X.; Zheng, Y.; Xu, Z.; Zhao, F.; Xiao, S. Characteristics of Target Crossing the Baseline in FSR: Experiment Results. *IEEE Geosci. Remote Sens. Lett.* **2023**, *20*, 3503105. [CrossRef]
13. Zheng, Y.; Ai, X.; Xu, Z.; Zhao, F.; Yang, Y. Parameter Estimation Based on Crossing Time Difference and Doppler Rate in FSR Network. *IEEE Geosci. Remote Sens. Lett.* **2022**, *19*, 4027105. [CrossRef]
14. Liu, M.; Zhang, Z.; Chen, Y.; Zheng, S.; Ge, J. Forward Scatter Radar Meets Satellite: Passive Sensing of Aerial Target Using Satellite Communication Waveforms. *Remote Sens.* **2022**, *14*, 1375. [CrossRef]

15. Colone, F. DVB-T-Based Passive Forward Scatter Radar: Inherent Limitations and Enabling Solutions. *IEEE Trans. Aerosp. Electron. Syst.* **2021**, *57*, 1084–1104. [CrossRef]
16. Contu, M.; De Luca, A.; Hristov, S.; Daniel, L.; Stove, A.; Gashinova, M.; Cherniakov, M.; Pastina, D.; Lombardo, P.; Baruzzi, A.; et al. Passive Multifrequency Forward-Scatter Radar Measurements of Airborne Targets Using Broadcasting Signals. *IEEE Trans. Aerosp. Electron. Syst.* **2017**, *53*, 1067–1087. [CrossRef]
17. Hamdollahzadeh, M.; Amiri, R.; Behnia, F. Moving Target Localization in Bistatic Forward Scatter Radars: Performance Study and Efficient Estimators. *IEEE Trans. Aerosp. Electron. Syst.* **2020**, *56*, 1582–1594. [CrossRef]
18. Kanona, M.E.A.; Ahmed, A.M.; Mirghani, M.E.; Hassan, M.K.; Abdalla, A.G.E.; Hamza, M.E. Performance Analysis of Hybrid Pre-Processing Techniques of Ground Target Classification in FSR using Neural Network. In Proceedings of the 2020 International Conference on Computer, Control, Electrical, and Electronics Engineering (ICCCEEE), Khartoum, Sudan, 26 February–1 March 2021.
19. Raja Abdullah, R.S.A.; Mohd Ali, A.; Rasid, M.F.A.; Abdul Rashid, N.E.; Ahmad Salah, A.; Munawar, A. Joint Time-Frequency Signal Processing Scheme in Forward Scattering Radar with a Rotational Transmitter. *Remote Sens.* **2016**, *8*, 1028. [CrossRef]
20. Hu, C.; Sizov, V.; Antoniou, M.; Gashinova, M.; Cherniakov, M. Optimal Signal Processing in Ground-Based Forward Scatter Micro Radars. *IEEE Trans. Aerosp. Electron. Syst.* **2012**, *48*, 3006–3026. [CrossRef]
21. Ustalli, N.; Lombardo, P.; Pastina, D. Detection Performance of a Forward Scatter Radar Using a Crystal Video Detector. *IEEE Trans. Aerosp. Electron. Syst.* **2018**, *54*, 1093–1114. [CrossRef]
22. Ustalli, N.; Lombardo, P.; Pastina, D. Generalized Likelihood Ratio Detection Schemes for Forward Scatter Radar. *IEEE Trans. Aerosp. Electron. Syst.* **2018**, *54*, 2951–2970. [CrossRef]
23. Liu, W.; Liu, J.; Hao, C.; Gao, Y.; Wang, Y.-L. Multichannel Adaptive Signal Detection: Basic Theory and Literature Review. *Sci. China Inf. Sci.* **2022**, *65*, 121301. [CrossRef]
24. Liu, W.; Liu, J.; Liu, T.; Chen, H.; Wang, Y.-L. Detector Design and Performance Analysis for Target Detection in Subspace Interference. *IEEE Signal Process. Lett.* **2023**, *30*, 618–622. [CrossRef]
25. Addabbo, P.; Besson, O.; Orlando, D.; Ricci, G. Adaptive Detection of Coherent Radar Targets in the Presence of Noise Jamming. *IEEE Trans. Signal Process.* **2019**, *67*, 6498–6510.
26. Orlando, D.; Ricci, G.; Scharf, L.L. A Unified Theory of Adaptive Subspace Detection Part I: Detector Designs. *IEEE Trans. Signal Process.* **2022**, *70*, 4925–4938. [CrossRef]
27. Xue, J.; Ma, M.; Liu, J.; Pan, M.; Xu, S.; Fang, J. Wald- and Rao-Based Detection for Maritime Radar Targets in Sea Clutter with Lognormal Texture. *IEEE Trans. Geosci. Remote Sens.* **2022**, *60*, 5119709. [CrossRef]
28. Sun, M.; Liu, W.; Liu, J.; Hao, C. Complex Parameter Rao Wald Gradient and Durbin Tests for Multichannel Signal Detection. *IEEE Trans. Signal Process.* **2021**, *70*, 117–131. [CrossRef]
29. Nomakuchi, K. A Note on The Uniformly Most Powerful Tests in The Presence of Nuisance Parameters. *Ann. Inst. Stat. Math.* **1992**, *44*, 141–145. [CrossRef]
30. Ciuonzo, D.; De Maio, A.; Orlando, D. A Unifying Framework for Adaptive Radar Detection in Homogeneous Plus Structured Interference—Part II: Detectors Design. *IEEE Trans. Signal Process.* **2016**, *64*, 2907–2919. [CrossRef]
31. Naderpour, M.; Ghobadzadeh, A.; Tadaion, A.; Gazor, S. Generalized Wald Test for Binary Composite Hypothesis Test. *IEEE Signal Process. Lett.* **2015**, *22*, 2239–2243. [CrossRef]
32. Wang, Z.; Li, G.; Chen, H. Adaptive Persymmetric Subspace Detectors in the Partially Homogeneous Environment. *IEEE Trans. Signal Process.* **2020**, *68*, 5178–5187. [CrossRef]
33. Shikhaliev, A.P.; Himed, B. GLR, Rao, and Wald Tests for Distributed Parametric Detection in Subspace Interference. *IEEE Trans. Signal Process.* **2023**, *71*, 388–400. [CrossRef]
34. Wang, Z.; Liu, J.; Li, Y.; Chen, H.; Peng, M. Adaptive Subspace Signal Detection in Structured Interference Plus Compound Gaussian Sea Clutter. *Remote Sens.* **2022**, *14*, 2274. [CrossRef]
35. Liu, J.; Li, J. Robust Detection in MIMO Radar with Steering Vector Mismatches. *IEEE Trans. Signal Process.* **2019**, *67*, 5270–5280. [CrossRef]
36. Jing, X.; Su, H.; Shen, L.; Mao, Z.; Jia, C. Adaptive Radar Detection in the Clutter and Noise Cover Pulse Jamming Environment. *Signal Process.* **2023**, *205*, 108852. [CrossRef]
37. Liu, J.; Zhou, W.; Zaimbashi, A.; Li, H. Persymmetric Adaptive Array Detection of Spread Spectrum Signals. *IEEE Trans. Inf. Theory* **2020**, *66*, 7828–7834. [CrossRef]
38. De Maio, A.; Han, S.; Orlando, D. Adaptive Radar Detectors Based on the Observed FIM. *IEEE Trans. Signal Process.* **2018**, *66*, 3838–3847. [CrossRef]
39. Xue, J.; Xu, S.; Liu, J. Persymmetric Detection of Radar Targets in Nonhomogeneous and Non-Gaussian Sea Clutter. *IEEE Trans. Geosci. Remote Sens.* **2022**, *60*, 5103709. [CrossRef]
40. Hjorungnes, A.; Gesbert, D. Complex-Valued Matrix Differentiation: Techniques and Key Results. *IEEE Trans. Signal Process.* **2007**, *55*, 2740–2746. [CrossRef]
41. De Maio, A. A New Derivation of the Adaptive Matched Filter. *IEEE Signal Process. Lett.* **2004**, *11*, 792–793. [CrossRef]
42. Kelly, E.J. An Adaptive Detection Algorithm. *IEEE Trans. Aerosp. Electron. Syst.* **1986**, *AES-22*, 115–127. [CrossRef]

43. De Maio, A. Rao Test for Adaptive Detection in Gaussian Interference with Unknown Covariance Matrix. *IEEE Trans. Signal Process.* **2007**, *55*, 3577–3584. [CrossRef]
44. Besson, O. Rao, Wald, and Gradient Tests for Adaptive Detection of Swerling I Targets. *IEEE Trans. Signal Process.* **2023**, *71*, 3043–3052. [CrossRef]